Optimizing Blood Pressure Estimation Using Multiple Features Extracted from PPG Signals

Geonwoo Ji, Denis Bernard

***Abstract*—Blood pressure monitoring is essential for the prevention of cardiovascular diseases (CVDs). In recent years, the World Health Organization (WHO) has reported that blood pressure is the major risk factor that cause death of people around the world. To minimize these kinds of hazards in the society the best way is to develop the methods for blood pressure monitoring in which the individuals can obtain the valuable information about their health condition. In this project, we propose a ResNet-50 architecture and apply it with a publicly available dataset called Multiparameter Intelligent Monitoring in Intensive Care II (MIMIC II) for blood pressure estimation (BP) based on PPG signal only. The model consists of 5 stages each with a convolution and Identity block. Each convolution block has 3 convolution layers and each identity block also has 3 convolution layers.**

The mean absolute error (MAE) and standard deviation (STD) of the proposed model were respectively 2.03 and 3.12 mmHg for diastolic blood pressure (DBP), and 3.61 and 5.66 mmHg for systolic blood pressure (SBP). The experimental results are in full compliance with the international standards of the Association for the Advancement of Medical Instrumentation (AAMI) and the British Hypertension Society (BHS). We conclude that the proposed ResNet-50 architecture for blood pressure estimation is accurate. The essential differentiator between our method and existing methods of BP estimation based on manual feature calculation is that our method also can extracts PPG features automatically using a deep learning model that can easily handle the complicated and tedious calculation.

***Index Terms*—Photoplethysmogram, Blood Pressure, Convolutional Neural Network, Fully Connected layer.**

I. Introduction

BLOOD pressure (BP) is a crucial physiological parameter that measures the force exerted by blood as it circulates within the arteries. It is commonly expressed in millimeters of mercury (mmHg) and described by two values: systolic pressure, which corresponds to the pressure during heart contractions, and diastolic pressure, which corresponds to the pressure when the heart is at rest. A healthy adult typically has a resting blood pressure around 120 mmHg systolic and 80 mmHg diastolic. The monitoring of blood pressure plays a vital role in the early detection of medical conditions, particularly cardiovascular disorders, which are a leading cause of mortality and morbidity worldwide.

Hypertension, or high blood pressure, is a significant risk factor for serious health problems such as stroke and heart attack. On the other hand, hypotension, or low blood pressure, can lead to dizziness, fainting, and can signal underlying heart, endocrine, or neurological issues. Therefore, regular blood pressure monitoring is critical for maintaining overall health. Continuous monitoring of blood pressure, along with other vital signs, allows for an accurate assessment of the patient's physiological state, early diagnosis of potential issues, and prediction of worsening conditions.

Various methods of blood pressure monitoring, both invasive and noninvasive, are currently in use. Invasive methods involve the insertion of an arterial line, which provides continuous high-accuracy blood pressure measurement. However, invasive measurements carry the risk of infection and other negative consequences that can increase morbidity. Noninvasive methods, such as using an oscillometry inflatable arm or wrist cuff, are commonly employed for blood pressure measurement. These approaches are less invasive but can be uncomfortable due to repetitive inflation and deflation. Additionally, mobility limitations imposed by the measurement equipment make them unsuitable for long-term ambulatory blood pressure monitoring.

To ensure the accuracy of noninvasive blood pressure measurement technologies, the Association for the Advancement of Medical Instrumentation (AAMI) has established guidelines. According to AAMI, the mean absolute difference (MAD) of noninvasive blood pressure measurements should not exceed 5 mmHg, and the standard deviation should not exceed 8 mmHg compared to a reference method [1]. However, studies have shown that home blood pressure measuring devices can be inaccurate in a significant percentage of patients, with differences of 5 mmHg or higher being common [2], [3]. Therefore, it is crucial for other noninvasive technologies to exhibit similar accuracy and reliability as home blood pressure measuring devices.

Photoplethysmography (PPG) is an optically obtained signal that can be utilized to detect blood volume changes in the microvascular bed of tissue. This signal is obtained by illuminating the skin and measuring changes in light absorption. In a clinical setting, PPG signals are often acquired using a pulse oximeter, while in an ambulatory setting, smartwatches or other mobile devices can capture these signals. PPG signals provide valuable information about cardiovascular parameters such as heart rate, blood oxygen saturation, and blood pressure. Due to its noninvasive nature, simplicity, and low cost, PPG has immense potential for various clinical applications [4]. It is considered a promising technology that could serve as a feasible alternative to invasive arterial blood pressure measurement. Studies have demonstrated a high correlation between PPG signals and arterial blood pressure in both

G. Ji and D. Bernard are with the Department of Future Convergence Technology, Soonchunhyang University, Asan 31538, South Korea.

Manuscript received April 19, 2005; revised August 26, 2015. This work was supported by Basic Science Research Program through the National Research Foundation of Korea (NRF) funded by the Ministry of Education (NRF-2020R1I1A3A04037409 11). This work was also supported by the Soonchunhyang University Research Fund.

the time and frequency domains [5]. However, PPG signals are susceptible to artifacts that can significantly affect measurement accuracy [6]. Therefore, it is crucial to thoroughly evaluate the quality of PPG signals when utilizing them for medical applications.

A. CONTRIBUTION

The contributions of this paper can be summarized as follows.

- We propose a ResNet-50 architecture consisting of 5 stages each with a convolution and Identity block. Each convolution block has 3 convolution layers and each identity block also has 3 convolution layers which operate directly on the PPG features to reduce information loss and effectively model the PPG-BP relationship.
- The goal of this work is to demonstrate how to use PPG signals to make continuous blood pressure monitoring easier for older or fragile individuals. To be more specific, we concentrate at feature extraction strategies in order to improve the accuracy of blood pressure estimation.
- We investigate the performance of machine learning algorithms, including traditional machine learning (Lasso, Ridge, ExtratreeRegressor, LGBM), and deep learning.

The remainder of this study is organized as follows. Section II evaluates the existing literature on blood pressure estimation using PPG signal. Section III discusses the proposed blood pressure estimation methodology used in this project, including the publicly available dataset used, pre-processing, feature extraction, machine learning algorithms, CNN variant algorithms, and the design of the proposed ResNet-50 model. Section IV details the experimental setup and the results. Section V presents some discussion and describes the remaining challenges, and Section VI concluded this work.

II. RELATED WORK

BP estimation using Photoplethysmogram (PPG) signal is a good example to demonstrate the benefit of the proposed ResNet-50 model. In recent years, significant research has been conducted on BP estimation based on PPG signal only. These works have demonstrated methods to perform BP estimation based on PPG features and raw PPG signal which are summarized as follows:

A. Feature-based estimation

Maqsood *et al.* divided feature extraction techniques into three subgroups, Group A included time-domain features, Group B statistical features and Group C frequency domain-based features [7]. They applied machine learning algorithms and deep learning models, they found that a gated recurrent unit (GRU) model and a Bi-LSTM architecture achieved the best performance for time-domain features for blood pressure estimation compared to other techniques.

Rong *et al.* proposed a multi-type feature fusion neural network model, which included two CNNs used to train the morphological and frequency spectrum features of the PPG signal, and one Bi-LSTM which was used to train the temporal features of the PPG signal data. The standard deviation (STD) and mean absolute error (MAE) of the fusion model for SBP were 7.25 mmHg and 5.59 mmHg, respectively, and 4.48 mmHg and 3.36 mmHg for DBP [8].

Wang *et al.* extracted 54 features from PPG signal that may be related to BP, and a feature selection method based on a filter-wrapper was used to reject irrelevant and redundant features [9]. The features that maximized correlation with BP were finally selected as BP-oriented improved feature subset (IFS) and trained with a least absolute shrinkage and selection operator long short-term memory (LASSO-LSTM) model to estimate BP from the IFS. The MAE and STD of their method for all 54 features were 6.95 ± 5.98 mmHg and 5.73 ± 4.97 mmHg for SBP and DBP, respectively, and the result of the selected 15 features were 4.95 ± 4.15 mmHg for SBP and 3.15 ± 2.47 mmHg for DBP.

Khalid *et al.* developed the traditional generic (trained with uncategorized BP) algorithm and two-step algorithm (specifically optimized for each BP category) using machine learning. A total of 16 features were extracted from PPG data and selected three features with high correlation for BP estimation. Their two-step method first classified samples into three categories (hypotensive, normotensive, and hypertensive), and then performed BP estimation for the three categories. Generally, the two-step algorithm achieved the mean and standard deviation of 0.07 ± 7.1 mmHg and -0.08 ± 6.0 mmHg in estimating SBP and DBP, respectively. Categorically, the two-step method also achieved standard accuracy of -0.7 ± 5.8 mmHg for normotensive and 1.7 ± 7.6 mmHg for hypertensive except hypotensive systolic BP which was -3.0 ± 8.2 mmHg [10]. El-Hajj and Kyriacou used an attention-based Bi-GRU model, they selected only seven features among 22 time-domain PPG features to perform blood pressure estimation and achieved a good accuracy [11].

Wang *et al.* presented a blood pressure prediction-based method on features [12]. In their research, feature extraction was done using the multitaper method (MTM), and BP estimation was achieved using an artificial neural network (ANN). Although the feature extraction strategy required a long computational time, the proposed method produces good accuracy, with MAE and STD of 4.02 ± 2.79 mmHg for SBP and 2.27 ± 1.82 mmHg for DBP. In addition, here below these are works that predict BP using a variety of human physiological signals. In contrast, however, obtaining many signals necessitates greater effort [13]–[17].

Liu *et al.* extracted 21 time-scale PPG features proposed by Kurylyak, as well as 14 more features derived from PPG's second derivative (SDPPG) [18]. SDPPG has been shown to detect aortic stiffness and compliance, which are closely related to BP [19], [20]. The authors applied support vector regression (SVR) to estimate BP and found that combining features enhanced accuracy.

Li *et al.* collected PPG signals from 7993 patients from the MIMIC II database, and the features of these signals were extracted using semi-classical signal analysis [21]. The patients' BPs were estimated using a feedforward neural network. The patients' SBP and DBP estimation results were 0.035 ± 6.448 and 0.025 ± 4.857 mmHg, respectively.

Kurylyal *et al.* employed the MIMIC database to train the ANN, and a total of over 15,000 pulsations were analyzed and 21 parameters including the times of systolic, diastolic parts and ratio between them were extracted from each of them. The mean and standard deviation of absolute error were 3.80 $\pm$ 3.46 mmHg for SBP and 2.21 $\pm$ 2.09 mmHg for DBP [22].

Hasanzadeh *et al.* extracted 19 features from each PPG cycle based on its morphology [23]. These features and the corresponding SBP and DBP values were used to train different regression models. Their approach lacked personalization, which may have caused the higher estimation errors obtained, because these features have a person-specific response to BP [24]. Many studies have employed various machine learning algorithms to estimate blood pressure using features derived from PPG [25], [23].

B. Raw signal-based estimation

Yen *et al.* used PPG signals 8 seconds in duration to be trained with a model designed with CNN and LSTM for BP estimation [26]. They conducted ten-fold cross-validation, and found to reveal the MAEs of participants' SBP, DBP, heart rate (HR), and mean arterial pressure (ABP) to be 2.54 $\pm$ 3.88, 1.59 $\pm$ 2.45, 1.62 $\pm$ 2.55, and 1.59 $\pm$ 2.34 mmHg, respectively.

Leitner *et al.* proposed a hybrid neural network architecture consisting of convolutional, recurrent, and fully connected layers that operated directly on raw PPG time series and provided BP estimation every 5 seconds [27]. Slapnivcar *et al.* experimented with a large publicly available dataset using a ResNet model to estimate BP and achieved results of 6.88 mmHg and 9.43 mmHg for both DBP and SBP respectively [28].

Schlesinger *et al.* presented two techniques (calibration-free and a Siamese neural network) to enable continuous and noninvasive cuffless BP estimation using PPG signals with CNN [29]. When trained and tested on the MIMIC-II database, the Siamese network achieved an MAE of 5.95 mmHg and 3.41 mmHg for SBP and DBP respectively.

Zhang *et al.* collected PPG signals and BP data from 19 participants from the University of Queensland Vital Signs Dataset [25]. The BP was continuously estimated using a support vector machine. The SBP and DBP of the participants were 11.64 $\pm$ 8.20 mmHg and 7.62 $\pm$ 6.78 mmHg, respectively.

According to the literature survey, we examined whether CNN models were applied more in estimating the BP using the raw PPG signal rather than the PPG features. In our research, we attempted to apply CNN variants (i.ee., VGG16, AlexNet, and GoogleNet) to investigate how well were able to process PPG features to estimate BP. In addition, we determined many existing methods extract PPG features (i.e., time domain features, frequency domain features, statistical features) from PPG signal for BP estimation using machine learning or deep learning. However, existing techniques were designed to estimate BP using only a single category of features (e.g., time-domain features only). We considered that a combination of distinguishable features could perform better with CNN or machine learning models. In this study, we demonstrate how ResNet-50 model can process PPG features to estimate BP. We also investigated a ResNet-50 model that exhibited excellent performance in BP estimation.

III. METHODS

In this section, we provide a detailed explanation of the proposed methodology, which encompasses several key components. These include the utilization of a public dataset, the acquisition of PPG and ABP data, as well as preprocessing, segmentation, and feature extraction techniques. We also introduce various machine learning algorithms, alongside well-known CNN-variants such as VGG16, AlexNet, and GoogleNet. Additionally, we present our own novel contribution, the Residual network (ResNet-50), which is a specific CNN architecture designed to enhance the accuracy and performance of blood pressure estimation.

A. Methodology

The methodology proposed for blood pressure (BP) estimation utilizing the photoplethysmography (PPG) signal involves six key steps. Firstly, a suitable dataset is selected for the study. Next, PPG and arterial blood pressure (ABP) data are acquired from the chosen dataset. The acquired signals undergo pre-processing to remove noise and artifacts. Subsequently, segmentation is performed to identify relevant segments within the signals. Feature vectors are then extracted from the segmented signals, allowing for the representation of important characteristics. Additionally, the raw PPG signal itself is considered as a valuable input. The methodology further incorporates the application of various machine learning algorithms and CNN variants, such as VGG16, AlexNet, and GoogleNet. Lastly, a Residual network (ResNet-50) is employed specifically for BP estimation. By following these six steps, the proposed methodology aims to accurately estimate blood pressure using the PPG signal, providing valuable insights for healthcare applications.

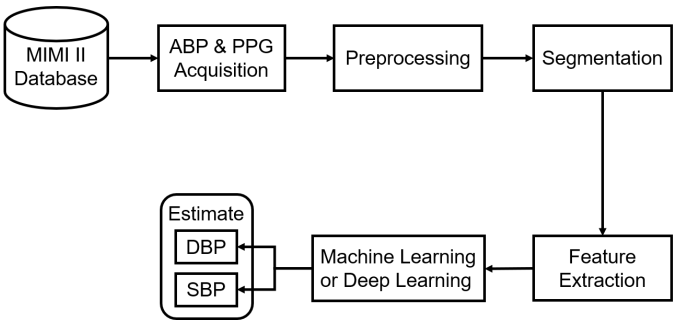

Fig. 1. Overview of the steps involved in the proposed BP estimation method. Each step is described in details here below.

1) Public dataset: To validate the feasibility of the proposed ResNet-50 model, a large and open database was required for training. The Multiparameter Intelligent Monitoring in Intensive Care II (MIMIC II) which is originally found from PhysioNet was adopted in this research. This dataset based on

MIMIC II database is also present in the University of California Irvine (UCI) Machine Learning Repository [30]. The dataset contain some physiological signals such as electrocardiogram (ECG) signals, photoplethysmography (PPG) signals and arterial blood pressure (ABP) sensor signals from 12,000 patients. These parameters were simultaneously measured at a sampling rate of 125 Hz. PPG and ABP signals were collected through fingertip and invasive measurements respectively [31]. ABP signals can indicate considerable information regarding cardiovascular functions; therefore, in this study, SBP and DBP were calculated based on ABP signals.

2) Acquisition of PPG and ABP: The dataset utilized in this study consisted of three physiological signals: photoplethysmography (PPG), electrocardiogram (ECG), and arterial blood pressure (ABP). These signals were organized and stored in a cell array of matrices, with each cell representing a distinct record. Each row within these matrices corresponded to a specific signal channel. For the purposes of this research, only the PPG and reference ABP signals from the MIMIC II dataset were extracted and employed.To identify the locations of the systolic and diastolic peaks, peak detection algorithms were applied to the ABP signals. This allowed us to precisely determine the sites of interest. The periodic ABP signal was subsequently partitioned into discrete interval segments, with each segment representing the maximum and lowest values within that interval. This process enabled the extraction of reference systolic blood pressure (SBP) and diastolic blood pressure (DBP) as target values for training and evaluation purposes.Simultaneously obtained PPG segments were also collected and utilized to derive training features. Once the peaks in the ABP signals were detected, the corresponding diastolic and systolic pressures were extracted and employed as crucial components within this project study.

3) Pre-processing: In order to categorize subjects appropriately, individuals with extremely high or significantly low blood pressure values were placed in a separate group. Specifically, diastolic blood pressure (DBP) values were required to be less than 130 and slightly larger than 60, while systolic blood pressure (SBP) values were expected to be less than 180 and greater than 80 [26]. By establishing these criteria, a more refined classification and analysis of blood pressure data was achieved.

It is worth noting that PPG waveforms in some individuals may exhibit irregularities and distortions due to various factors such as changes in sensor position or movement. These irregularities can significantly affect the extraction of meaningful features from the PPG signals. Figure 2 provides a visual representation of a diverse range of irregular PPG wave patterns that can be encountered. It is important to acknowledge and account for these variations in order to ensure accurate and reliable PPG feature extraction.

Furthermore, it is not uncommon for certain participants to exhibit abnormal blood pressure waveform signals due to factors such as the influence of medication, sensor movement, or other circumstances. These factors can introduce additional complexities and challenges in the analysis and interpretation of blood pressure data. Therefore, it is crucial to carefully consider and address these potential confounding factors when conducting research or clinical assessments involving blood pressure estimation.

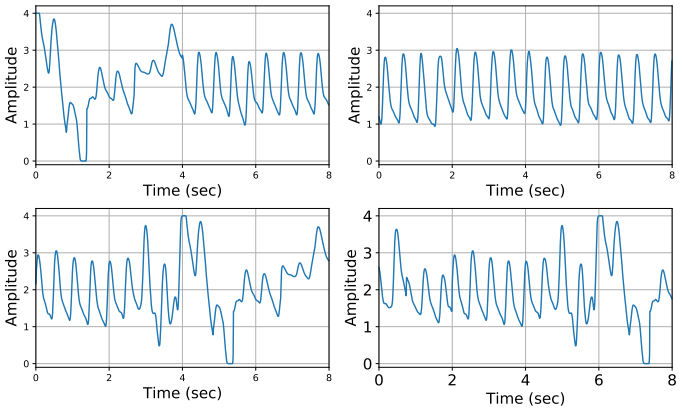

Fig. 2. 8 second windows of inappropriate PPG signals.

4) Segmentation: In order to extract relevant information from the raw PPG data, a sliding window approach was employed, where an 8-second window with a 2-second overlap was applied to the PPG signal [26]. This windowing technique facilitated the analysis of successive segments of the PPG signal, allowing for the examination of temporal variations and patterns.

The control of blood pressure in operating rooms and intensive care units often involves the manual adjustment of vasopressor medication to maintain an optimal mean arterial pressure (MAP) range. Ideally, changes in vasopressor infusion rates should be initiated promptly upon detecting alterations in blood pressure measurements. This study presents novel experimental evidence demonstrating the feasibility of estimating blood pressure changes in the operating room setting, even when dealing with irregular and distorted PPG signals resulting from changes in sensor position or movement, which are common occurrences in many patients.

The project encompassed a diverse range of PPG signals, including those that were notably ambiguous and challenging to interpret. Fig. 3 showcases examples of PPG signals with favorable characteristics that were utilized in the study. By incorporating such signals, the investigation aimed to evaluate the effectiveness of estimating blood pressure fluctuations using real-world data that accurately reflected the complexities encountered in clinical scenarios.

5) Feature Extraction: In this study, we introduce a novel approach for estimating diastolic blood pressure (DBP) and systolic blood pressure (SBP) solely based on the analysis of the photoplethysmography (PPG) signal, without considering its shape as either appropriate or inappropriate. Our proposed algorithm leverages features extracted from the signal within specific time intervals. Various domains, including time, frequency, gradient, statistical, amplitude, and morphological, are explored to extract informative features from the PPG signal, as documented in [9]. These features are computed using an 8-second PPG window with a stride of 2 seconds to ensure overlap and capture precise temporal information.

Within each 8-second PPG window, a total of 82 features are extracted. Among these features, the slope points, dias-

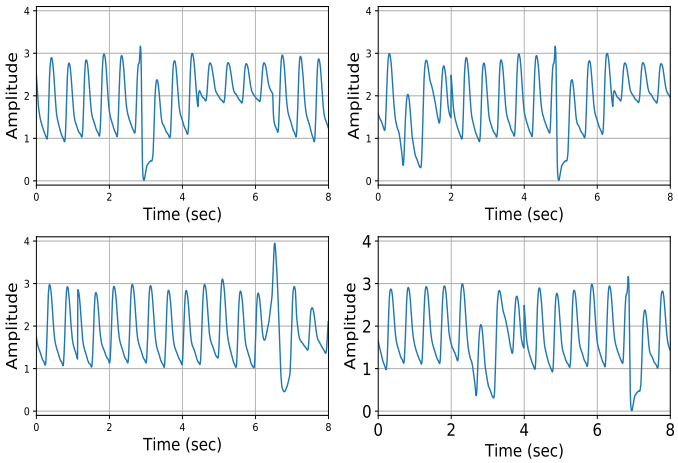

Fig. 3. 8 second windows of inappropriate PPG signals that were applied to this work.

tolic peak, inflection point, and systolic peak hold significant importance for accurate feature extraction from PPG signals. These key aspects capture essential characteristics of the PPG waveform, such as the rate of change, the points of maximum and minimum values, and critical landmarks associated with the cardiac cycle

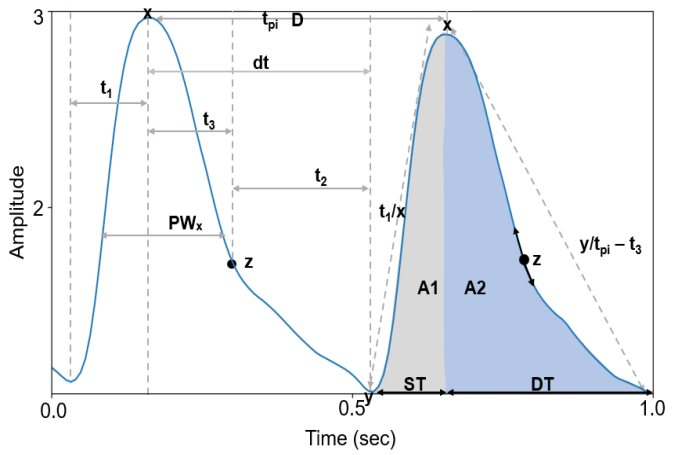

Fig. 4. Depicts the morphologies of the PPG signal from which 82 features were extracted.

1) Morphological features: In this study, the following morphological features were extracted from PPG signals according to cardiovascular status in Fig. 4.
   - Systolic peak: A direct pressure wave originating from the left ventricle and propagating towards the body's periphery causes a systolic peak. This peak signifies the highest point of arterial pressure during each cardiac cycle. It serves as a crucial indicator of the force exerted by the heart as it contracts and pushes blood into the arteries. The systolic peak is represented by feature x.
   - Diastolic peak: It is generated by pressure wave reflections in the arteries of the lower body. These reflections occur during the diastolic phase and provide valuable insights into vascular function and arterial stiffness. The diastolic peak is represented by feature y.
   - Dicrotic notch: In the central arteries, the dicrotic notch is a conspicuous and distinguishing characteristic of a pressure waveform. In these arteries, it is universally employed to mark the end of systole and start of diastole. The dicrotic notch is represented by characteristic z.
2) Gradient-based features: The extraction of these features relied on analyzing the slopes of the ascending and descending branches, as well as the accelerations associated with these branches. The slopes of the signal are closely linked to pulse velocity, offering valuable insights into cardiovascular dynamics. Notable features encompass the rising slope of the systolic peak and the falling slope of the diastolic peak, which provide crucial information about the arterial waveform characteristics.
3) Time-based features: Typically, the inverse of the systolic and diastolic peak times is used to gauge the stiffness of large arteries. In addition to pulse width, another measure known as systemic vascular resistance (SVR) is the inverse of the time interval between the systolic peak and the inflection point, as well as the systolic peak and diaphragmatic notch. Additionally, the crest time is calculated from the minimum point to the systolic peak. The time-based features included, diastolic peak time, dicrotic notch time, systolic peak time, time between systolic and diastolic peaks, pulse interval, and other derivative features, as shown in Table I.
4) Amplitude-based features: Amplitude-based features encompass metrics such as the augmentation index, relative augmentation index, peak distance, inflection point area ratio, systolic area, and diastolic area. These features provide valuable information about the magnitude and shape of the arterial waveform. They offer insights into arterial stiffness, wave reflection, temporal separation between peaks, relative contribution of the inflection point, and areas under the systolic and diastolic portions of the waveform.
5) Statistical features: We aimed to extract morphological information from a single-window PPG signal by analyzing statistical parameters and their correlation with the target variable. We evaluated various statistical measures, including mean, median, standard deviation, root-mean-square, sum, variance, eigenvalue summation, eigenvalues, and percentiles (PWx; where x = 5, 10, 25, 33, 50, 66, 75, 90, 95). By examining these statistical features, we obtained valuable insights into the characteristics and trends of the PPG signal, enabling us to establish their relationship with the target variable.
6) Frequency domain features: To capture frequency domain characteristics, we utilized power spectral density (PSD), harmonic frequency, fundamental component frequency, and fundamental component magnitude. The harmonic frequency features encompassed the 2^{nd} harmonic frequency, 2nd harmonic magnitude, 3^{rd} harmonic frequency, and 3^{rd} harmonic magnitude. Additionally,

TABLE I
DEFINITION OF EXTRACTED FEATURES

Features List					
Gradient-based Features			**Statistical Features**		
No	**Symbol**	**Description**	**No**	**Symbol**	**Description**
1	t_1/x	Systolic peak rising slope	42	Auto-correlation index [0]	Previous and next window correlation
2	$y/(t_{pi}-t_3)$	Diastolic peak falling slope	43	Auto-correlation index [1]	Previous and next window correlation
Time-based Features			44	Auto-correlation index [2]	Previous and next window correlation
3	t_2	Diastolic peak time	45	Auto-correlation index [3]	Previous and next window correlation
4	t_3	Dicrotic notch time	46	Auto-correlation index [4]	Previous and next window correlation
5	t_1/t_{pi}	Time domain derivative	47	Auto-correlation index [5]	Previous and next window correlation
6	dt	Time between systolic and diastolic peaks	48	entropy	Entropy
7	e_2	2^{nd} discrete difference-maximum-index [1]	49	mean crossing indices	Mean crossing indices
8	t_1	Systolic peak time	50	no mean crossings	No mean crossings
9	t_2/t_{pi}	Time domain derivative	51	eig max	Eigenvalue values
10	t_3/t_{pi}	Time domain derivative	52	eig min	Eigenvalue values
11	dt/t_{pi}	Time domain derivative	53	Minimum correlation	Window correlation values
12	t_{a1}	9^{th} discrete difference max index [0] / sampling rate	54	Mean correlation	Window correlation values
13	t_{b1}	9^{th} discrete difference min index [0] / sampling rate	55	maximum correlation	Window correlation values
14	t_{e1}	9^{th} discrete difference max index [1] / sampling rate	56	eig sum	Summation eigenvalue values
15	t_{f1}	9^{th} discrete difference min index [1] / sampling rate	57	Sum A_1	Systolic Area values
16	b_2/a_2	2^{nd} discrete difference max index [0]/ min index [0]	58	Sum A_2	Diastolic Area values
17	e_2/a_2	Time domain derivative	59	rsm	Root mean square
18	$(b_2+e_2)/a_2$	Time domain derivative	60	sum	Summation
19	t_{a2}	Time domain derivative	61	var	Variance
20	t_{b2}	Time domain derivative	62	std	Standard deviation
21	t_{a1}/t_{pi}	Time domain derivative	63	mean	Mean
22	t_{b1}/t_{pi}	Time domain derivative	64	sm	Scaled wave mean
23	t_{f1}/t_{pi}	Time domain derivative	65	median	Median
24	t_{a2}/t_{pi}	Time domain derivative	66	PW_{90}	Percentile 90
25	t_{b2}/t_{pi}	Time domain derivative	67	PW_{75}	Percentile 75
26	$(t_{a1}+t_{a2})/t_{pi}$	Time domain derivative	68	PW_{66}	Percentile 66
27	$(t_{b1}+t_{b2})/t_{pi}$	Time domain derivative	69	PW_{50}	Percentile 50
28	$(t_{e1}+t_2)/t_{pi}$	Time domain derivative	70	PW_{33}	Percentile 33
29	$(t_{f1}+t_3)/t_{pi}$	Time domain derivative	71	PW_{25}	Percentile 25
30	t_{pi}	Pulse interval	72	PW_{10}	Percentile 10
Frequency-based Features			73	PW_5	Percentile 5
31	f_{base}	Fundamental component frequency	74	PW_{95}	Percentile 95
32	$\|s_{base}\|$	Fundamental component magnitude	**Amplitude-based Features**		
33	f_2	2^{nd} harmonic frequency	75	y/x	Augmentation index
34	$\|s_2\|$	2^{nd} harmonic magnitude	76	x-y/x	Relative augmentation index
35	f_3	3^{nd} harmonic frequency	77	z/x	Amplitude derivative
36	$\|s_3\|$	3^{nd} harmonic magnitude	78	y-z/x	Amplitude derivative
37	sqr PSD	Square root PSD values	79	D	Peak distance
38	mean PSD	Mean PSD values	80	A_2/A_1	Inflection point area ratio
Morphological Features			81	A_1	Systolic area
39	z	Dicrotic notch	82	A_2	Diastolic area
40	x	Systolic peak			
41	y	Diastolic peak			

mean PSD values and square root PSD values were incorporated as PSD features. Estimation of the power spectral density was performed using a periodogram method. These frequency domain features provided valuable insights into the distribution and strength of different frequency components present in the PPG signal, enabling a comprehensive analysis of its spectral characteristics.

B. Machine Learning Algorithms

Below, we present the extensive range of machine learning models investigated in this study to explore the potential relationship between input features and blood pressure. Once the features were extracted, we employed a diverse set of machine learning algorithms to estimate systolic and diastolic blood pressure. The training process involved utilizing the 82 extracted features to build and train multiple models. These models were designed to analyze the input features and learn patterns that could effectively predict blood pressure values. To estimate SBP and DBP, separate models were trained, their parameters are listed in the Table II. The performance of each machine-learning model was recorded.

1) Light gradient boosting machine (LightGBM): This gradient-boosting framework uses a tree-based learning method. However, what sets it apart from other tree-based algorithms is the vertical expansion of the tree structure, as opposed to the horizontal expansion. This means that LightGBM operates in a leaf-by-leaf manner, while other algorithms follow a level-by-level approach.

By expanding the tree structure vertically, LightGBM aims to optimize the learning process and enhance its predictive capabilities. This unique characteristic of LightGBM enables it to capture more intricate patterns and relationships within the data, potentially leading to improved performance in various prediction tasks.

2) Extremely randomized tree regressor (extra tree regressor): Predictive analysis is one of the most effective machine-learning methods. Even when features have a non-linear relationship with targets, they perform well in estimating output. By merging the predictions of each decision tree, random forest also lowers overfitting, which is it reduces the variance-bias trade-off. The robustness of the model was determined by the diversity of each tree. The regression model was constructed with the Sci-kit learn library.
3) Ridge regression: This approach is commonly known as regularization, which extends the ordinary least square loss function by adding a penalty term to the parameter estimations. The objective is not only to minimize the sum of squared residuals but also to constrain the magnitude of the parameter estimates, effectively reducing them towards zero. As the complexity of the model increases, the parameter estimates tend to grow exponentially. By imposing constraints on the model coefficients, we can effectively limit the model's complexity, preventing overfitting and improving its generalization performance. This regularization technique aids in controlling the trade-off between model complexity and goodness-of-fit, ultimately leading to more robust and interpretable models.
4) Lasso regression: Lasso regression is a coefficient shrinkage method used in linear regression models. Unlike ridge regression, which penalizes the sum of squares of the coefficients, lasso regression penalizes the L1 norm of the coefficients, which is the sum of their absolute values. This L1 penalty encourages sparsity in the coefficient estimates, effectively setting some coefficients to exactly zero. As a result, lasso regression tends to select a subset of the most important features, leading to a more interpretable and potentially more accurate model. This difference in penalty between lasso and ridge regression makes lasso particularly useful in scenarios where feature selection and model interpretability are desired.

TABLE II
MACHINE LEARNING MODEL PARAMETERS

Machine learning models	
Model	Specifications
LightGBM	boosting_type = "goss", num_leaves=3000, learning_rate=0.05, min_child_weight=0.002, n_estimators=300, random_state=42, n_jobs=-1
Ridge	alpha = 1, solver= 'cholesky', random_state=33
Lasso	alpha=1.0, max_iter=1000, random_state=33, tol=0.0001
Extra tree	n_estimators=100, min_samples_split=2, n_jobs= -1, min_samples_leaf=1, random_state=42

C. CNN Variant Algorithms

CNN models have a remarkable capability to leverage spatial or temporal correlations present in data. They employ a series of learning phases that consist of convolutional layers, nonlinear processing units, and sub-sampling layers. The CNN architecture follows a feedforward approach, with each layer utilizing a set of convolutional kernels to perform diverse transformations. Through the convolution operation, valuable characteristics can be extracted from data points that exhibit spatial relationships. In this study, we evaluated the effectiveness of different CNN variants trained on 82 features extracted from the PPG signal, aiming to assess their performance.

1) AlexNet: It comprises five convolutional layers, initialized with an 11x11 kernel. It introduced the utilization of max-pooling layers, rectified linear unit (ReLU) activation functions, and dropout in its three dense layers. Through this network, the estimation of SBP and DBP was performed.
2) VGG16: VGG16 is a relatively older type of convolutional neural network based on research on the densification of such networks. The network employs small 3 x 3 filters. In addition, the network is characterized by its simplicity, with only pooling layers and a fully linked layer serving as additional components.
3) GoogLeNet: It is developed by Google as an advancement of the LeNet architecture, incorporates the revolutionary inception module, which serves as the network's core framework. With 22 layers, GoogLeNet is a deep convolutional neural network that builds upon the foundation of the inception network. The inception module revolutionizes information capturing by integrating parallel filter sizes, allowing the network to effectively capture details across various spatial scales.

D. Design of a proposed Residual Network (ResNet-50)

The proposed model consists of multiple blocks, each serving a specific purpose in the overall architecture. The model begins with a convolutional block that performs a convolution operation on the input data. This block applies a set of filters to extract features from the input. It is followed by the identity block which act as a key component of ResNet-50. It consists of three convolutional layers with shortcut connections. The shortcut connection bypasses the middle convolutional layer and directly adds the input to the output, allowing the model to learn residual mappings. After that it is followed by the Convolutional Block with Projection Shortcut, this block is similar to the identity block but includes a projection shortcut to match the dimensions of the input and output. It uses a 1x1 convolutional layer to project the input if the dimensions are not compatible. Then, the convolutional block and identity block are repeated several times, creating multiple stacked layers in the model. These repeated blocks allow for deeper and more complex feature extraction. At the end of the ResNet-50 model, a global average pooling layer is applied to reduce the spatial dimensions of the output feature map. It computes the average value of each feature map, resulting in a fixed-length feature vector. Finally, the global average

pooling layer is followed by a fully connected layer that maps the extracted features to the desired output classes or regression values. This layer combines the information from the previous layers and performs the final regression (SBP and DBP Estimation).

IV. Experiments and Results

As mentioned in Section III-A1, we used a dataset from the UCI Machine Learning Repository based on MIMIC II. We used several criteria developed by other researchers to perform computations based on ABP signals, the signals with SBP $\geq$ 180, SBP $\leq$ 80, DBP $\geq$ 130, DBP $\leq$ 60 were excluded from this study [16], [26], [31]. A total of 912 subjects remained after preprocessing and 82 features were extracted from the PPG signal. Each of the derived features yielded a total of 203,431 samples or instances, accounting for approximately 7.6% of the dataset. We employed the extracted features to train our proposed ResNet-50 model, machine learning algorithms and other CNN variant algorithms (i.e., VGG16, AlexNet, and GoogleNet).

A. Experiment Setting

We used the Python programming language to implement our algorithms and conduct experiments. The neural network model was developed using the Keras library with the TensorFlow backend. To estimate the BP using the extracted features and raw PPG signal, all experiments were conducted using a Nvidia Jetson AGX Xavier. This computer had a GPU (a 512-core Volta GPU with tensor cores), which helped us run our experiments more in less time. It also had a CPU (8-core ARM v8.2 64-bit CPU, 8MB L2 + 4MB L3), memory (32GB 256-Bit LPDDR4x or 137GB/s), and storage of 32GB eMMC 5.1. All networks were trained using the Adam optimizer and all 82 features were selected for use in our experiments, and 10-fold cross validation was carried out for each experiment.

B. Performance Evaluation Metrics

The performance evaluation of the BP estimation model involved the calculation of four key metrics: mean error (ME), mean absolute error (MAE), root mean squared error (RMSE), and standard deviation (STD). These metrics provided a comprehensive assessment of the disparity between the estimated and reference BP values. The formulas for calculating these metrics are shown in Equations (1)-(4).

$$ME = \frac{1}{N}\sum_{i=1}^{N}(y_i - \hat{y}_i) \tag{1}$$

$$STD = \sqrt{\frac{1}{N}\sum_{i=1}^{N}(x_i - ME)^2} \tag{2}$$

$$MAE = \frac{1}{N}\sum_{i=1}^{N}|y_i - \hat{y}_i| \tag{3}$$

$$RMSE = \sqrt{\frac{1}{N}\sum_{i=1}^{N}(y_i - \hat{y}_i)^2} \tag{4}$$

where y_i is the actual value, $\hat{y}_i$ is the estimated value, N is the number of data and x_i is the error between the actual and the estimated values.

C. Performance of Machine Learning Models and CNN Variants

We conducted several experiments involving different machine learning models and variants of CNNs. In these experiments, we utilized all 82 extracted features from the PPG signals as input to train our models. For a while now, machine learning algorithms have been employed with successful features. In our experiments, we employed all the features in both machine learning and CNN variants, and assessed their performance. The extra tree regressor performed better than the other machine learning methods, and the ResNet-50 model outperformed other CNN variants.

The experimental results are summarized in Tables III and IV. The machine learning algorithms were expected to show lower MAEs than the CNN variants, but the results provide additional information that CNN variants also performed very well with features, whereas the standard machine learning techniques are showed a significant decrease. For instance, the tables show that AlexNet outperformed the ExtraTreesRegressor by an MAE gap of 1.21 mmHg and 3.97 mmHg for DBP and SBP, respectively.

TABLE III
MACHINE LEARNING ALGORITHMS RESULTS

ML Models	DBP (mmHg)		SBP (mmHg)	
	MAE ± STD	RMSE	MAE ± STD	RMSE
Extra Tree	**3.83 ± 5.70**	**5.73**	**8.81 ± 12.73**	**12.74**
LightGBM	3.84 ± 5.72	5.71	8.98 ± 12.75	12.76
Lasso	6.82 ± 8.66	8.69	17.29 ± 20.94	20.99
Ridge	6.48 ± 8.36	8.40	16.00 ± 19.49	19.53

TABLE IV
CNN VARIANT ALGORITHMS RESULTS

CNN Variants	DBP (mmHg)		SBP (mmHg)	
	MAE ± STD	RMSE	MAE ± STD	RMSE
AlexNet	2.62 ± 11.89	11.90	4.84 ± 24.94	25.00
VGG16	4.28 ± 6.21	6.26	8.72 ± 12.72	12.85
GoogLeNet	3.09 ± 4.61	4.63	4.72 ± 7.52	7.54

D. Performance of the Proposed Residue Network (ResNet-50)

The proposed ResNet-50 model was trained using the features extracted from the PPG signals. We attempted to apply different number of epochs and learning rates to train our model: - in each experiment a 10-fold cross validation was performed for BP estimation. From the experiments we observed that, the ResNet-50 model trained with large number of epochs and the learning rate of 0.0001 performed very well and provided the best results as shown in the Table V.

Fig.6 shows the learning curve of the ResNet-50 performance for BP estimation. The plot of training loss decreased to a point of stability, and the plot of validation loss shows a decrease; however, there was a gap between the validation loss and the training loss.

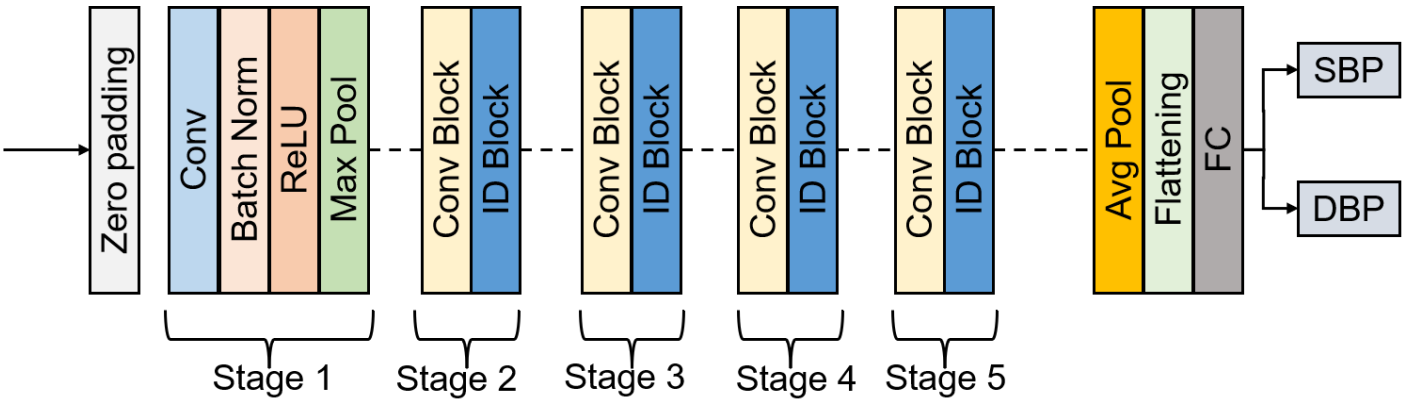

Fig. 5. The architecture of the proposed ResNet-50 model.

TABLE V
THE RESULTS OF A PROPOSED MODEL BY APPLYING DIFFERENT NUMBER OF EPOCHS AND LEARNING RATES

	DBP (mmHg)		SBP (mmHg)	
Proposed Model	MAE ± STD	RMSE	MAE ± STD	RMSE
ResNet-50 number of epochs = 30 and learning rate = 0.001	4.48 ± 5.01	5.07	5.69 ± 6.17	6.34
ResNet-50 number of epochs = 50, and learning rate = 0.0001	4.02 ± 4.55	4.86	4.52± 5.12	5.67
ResNet-50 number of epochs = 100 and learning rate = 0.0001	3.15 ± 3.36	3.68	3.97 ± 4.02	4.39
ResNet-50 number of epochs = 150 and learning rate = 0.0001	**2.03 ± 3.12**	**3.15**	**3.61 ± 5.66**	**5.70**

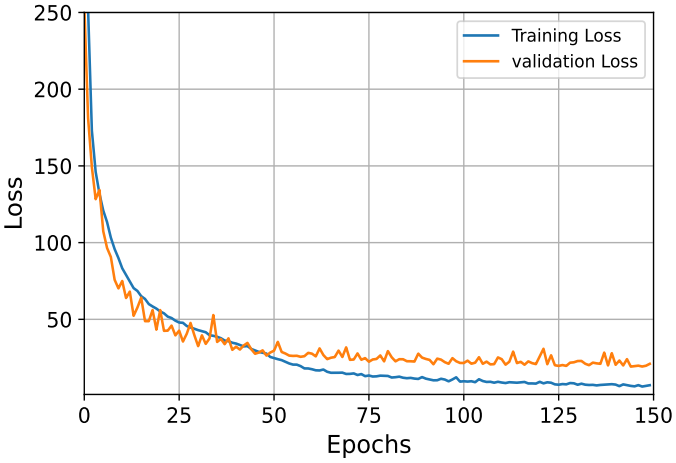

Fig. 6. Loss functions for the training and validation processes.

E. Comparison of Our Results with Other Existing Work

To verify the accuracy of the proposed ResNet-50 model, we compared its performance with that of the models used in previous relevant studies. Table VI shows that the MAEs of DBP and SBP obtained using the proposed model were smaller than those obtained in previous studies. However, the STDs of DBP and SBP obtained with our ResNet-50 model seem to have a slightly larger error compared to the few related studies. The STDs gap between our work and the previous study with low STDs error were 2.93 mmHg and 5.6 mmHg for DBP and SBP, respectively. Owing to our profound results, this finding indicates that the proposed model can estimate BP more accurately.

F. Comparison with International Standards

In this section, we compare the experimental results of our proposed model with two international standards: - the Association for the Advancement of Medical Instrumentation (AAMI) [32] and the British Hypertension Society (BHS) [33].

The BHS standard grades blood pressure (BP) measurement devices based on their cumulative percentage of error under their different thresholds, which is 5, 10, and 15 mmHg. This standard includes grades A, B and C. It can be seen from Table VII that, both the SBP and DBP estimated using the proposed model achieved grade A. We concluded from the table that the model proposed in this study conforms to the BHS international standards.

The Association for the Advancement of Medical Instrumentation (AAMI) is based on mean error (ME) and standard deviation (STD). According to the standard, the ME and STD had to be less than 5 mmHg and 8 mmHg for the DBP and SBP, respectively. From Table VIII, it may be observed that, the ME of DBP and SBP were 0.91 mmHg and 1.15 mmHg respectively. They were both less than 5 mmHg. The STD of DBP and SBP were 1.68 mmHg and 2.43 mmHg, respectively, which were both less than 8 mmHg. These results are in agreement with the AAMI international standards, as shown in Table VIII.

V. DISCUSSION AND REMAINING CHALLENGES

Table VI lists the state-of-the-art related to this study. Rong *et al.* trained the morphological and frequency spectrum features of PPG signal using a CNN and the temporal features of PPG signal using a Bi-LSTM model. Despite the fact that their method automatically extracts PPG features and their results were consistent with BHS international standards, the errors

TABLE VI
PERFORMANCE COMPARISON WITH RELATED WORK

Authors	Approach	Dataset	Model	DBP (mmHg) MAE ± STD	SBP (mmHg) MAE ± STD
Rong *et al.* [8]	PPG	UCI (MIMIC II)	MTFF-ANN (2CNN+1 LSTM)	3.36 ± 4.48	5.59 ± 7.25
Wang *et al.* [9]	PPG	UCI (MIMIC II)	LASSO-LSTM	3.15 ± 2.47	4.95 ± 4.15
Wang *et al.* [12]	PPG	MIMIC	ANN	2.27 ± 1.82	4.02 ± 2.79
Panwar *et al.* [16]	PPG	UCI (MIMIC II)	LRCN	2.30 ± 0.19	3.97 ± 0.06
Hasanzadeh *et al.* [23]	PPG	UCI (MIMIC II)	AdaBoost	4.17 ± 4.22	8.22 ± 10.38
This work	**PPG**	**UCI (MIMIC II)**	**ResNet-50**	**2.03 ± 3.12**	**3.15 ± 5.66**

TABLE VII
COMPARISON WITH THE BHS STANDARD

		Cumulative Percentage Error		
		$\leq$ 5 mmHg	$\leq$ 10 mmHg	$\leq$ 15 mmHg
BHS [33]	Grade A	60%	85%	95%
	Grade B	50%	75%	90%
	Grade C	40%	65%	85%
Our Results	DBP	85.5%	90.5%	92.8%
	SBP	82.4%	89.3%	91.6%

TABLE VIII
COMPARISON WITH THE AAMI STANDARD

		ME (mmHg)	STD (mmHg)	Subjects
AAMI [32]	DBP & SBP	$\leq$ 5	$\leq$ 8	$\geq$ 85
Our Results	DBP	0.91	1.68	912
	SBP	1.15	2.43	912

were still slightly large [8]. Wang *et al.* extracted 54 features from PPG signal that may be associated with BP and a filter-wrapper cooperative feature selection method was utilized to remove irrelevant and redundant features. The features that maximize the correlation with BP were finally selected as a BP-oriented improved feature subset (IFS), and trained with a LASSO-LSTM model to estimate blood pressure from the IFS. Although their results were satisfactory, it was subject to the same problem of the complexity of manually extracting features [9].

Although the majority of the predicted results were acceptable, a small percentage exhibited high errors because the UCI dataset primarily consisted of clinical data collected from hospitals' ICUs (Intensive Care Units). Drugs that induced abnormal increases in blood pressure were found in almost all samples.As a result, some blood pressure predictions have large errors.

The proposed RenNet-50 model is a generic model with no personalized calibration for individuals. The continuous collection of personal BP and PPG data is required to fine-tune the deep learning model to fit individual demands. As a result, the model was the most accurate at estimating personal blood pressure.

In our experiments, we used an Nvidia Jetson Nano and AGX to run our BP estimation algorithms. The machine learning algorithms, CNN variants (VGG16, AlexNet and GoogleNet), and the proposed ResNet-50 model required less than 15min, 1h, and 1h to perform training respectively.

VI. CONCLUSION

In this project, we present an effective ResNet-50 architecture for BP estimation using the PPG signal only. The designed ResNet-50 model comprised of 5 stages each with a convolution and Identity block. Each convolution block has 3 convolution layers and each identity block also has 3 convolution layers.The feutures extracted from PPG signal were used to train the proposed ResNet-50 model to estimate blood pressure (systolic and diastolic pressures).

Our proposed ResNet-50 model achieved the MAE and STD of 2.03 ± 3.12 mmHg for SBP and 3.61 ± 5.66 mmHg for DBP, respectively. These experimental results show that the proposed model can accurately estimate the blood pressure. Also, the results in terms of model correctness are better than the previously published methods, and they met the Grade A standard for both the BHS grading scale and the AAMI international standards.

Ultimately, using the PPG signal to achieve continuous blood pressure measurement is a very promising method. The growing population of hypertensive people requires this method. In the future, convenient and continuous blood pressure monitoring equipment will be the main focus of development. The proposed model will assist people in keeping track of their blood pressure on a daily basis.

REFERENCES

[1] A. N. Standard, "Ansi/aami/iso 81060-2: 2013. non-invasive sphygmomanometers. part 2: clinical investigation of automated measurement type," 2013.

[2] C. E. Evans, R. B. Haynes, C. H. Goldsmith, and S. A. Hewson, "Home blood pressure-measuring devices: a comparative study of accuracy." *Journal of hypertension*, vol. 7, no. 2, pp. 133–142, 1989.

[3] D.Pendick, "Some home blood pressure monitors aren't accurate https://www.health.harvard.edu/blog/home-blood-pressure-monitors-arent-accurate-201410297494," 2019.

[4] J. Allen, "Photoplethysmography and its application in clinical physiological measurement," *Physiological measurement*, vol. 28, no. 3, p. R1, 2007.

[5] G. Martínez, N. Howard, D. Abbott, K. Lim, R. Ward, and M. Elgendi, "Can photoplethysmography replace arterial blood pressure in the assessment of blood pressure?" *Journal of clinical medicine*, vol. 7, no. 10, p. 316, 2018.

[6] M. Elgendi, "Optimal signal quality index for photoplethysmogram signals," *Bioengineering*, vol. 3, no. 4, p. 21, 2016.

[7] S. Maqsood, S. Xu, M. Springer, and R. Mohawesh, "A benchmark study of machine learning for analysis of signal feature extraction techniques for blood pressure estimation using photoplethysmography (ppg)," *IEEE Access*, vol. 9, pp. 138 817–138 833, 2021.

[8] M. Rong and K. Li, "A multi-type features fusion neural network for blood pressure prediction based on photoplethysmography," *Biomedical Signal Processing and Control*, vol. 68, p. 102772, 2021. [Online]. Available: https://www.sciencedirect.com/science/article/pii/S1746809421003694

[9] D. Wang, X. Yang, X. Liu, L. Ma, L. Li, and W. Wang, "Photoplethysmography-based blood pressure estimation combining filter-wrapper collaborated feature selection with lasso-lstm model," *IEEE Transactions on Instrumentation and Measurement*, vol. 70, pp. 1–14, 2021.

[10] S. G. Khalid, H. Liu, T. Zia, J. Zhang, F. Chen, and D. Zheng, "Cuffless blood pressure estimation using single channel photoplethysmography: a two-step method," *IEEE Access*, vol. 8, pp. 58 146–58 154, 2020.

[11] C. El-Hajj and P. A. Kyriacou, "Deep learning models for cuffless blood pressure monitoring from ppg signals using attention mechanism," *Biomedical Signal Processing and Control*, vol. 65, p. 102301, 2021.

[12] L. Wang, W. Zhou, Y. Xing, and X. Zhou, "A novel neural network model for blood pressure estimation using photoplethesmography without electrocardiogram," *Journal of healthcare engineering*, vol. 2018, 2018.

[13] J. Esmaelpoor, M. H. Moradi, and A. Kadkhodamohammadi, "A multistage deep neural network model for blood pressure estimation using photoplethysmogram signals," *Computers in Biology and Medicine*, vol. 120, p. 103719, 2020.

[14] Y.-H. Li, L. N. Harfiya, K. Purwandari, and Y.-D. Lin, "Real-time cuffless continuous blood pressure estimation using deep learning model," *Sensors*, vol. 20, no. 19, p. 5606, 2020.

[15] H. Eom, D. Lee, S. Han, Y. S. Hariyani, Y. Lim, I. Sohn, K. Park, and C. Park, "End-to-end deep learning architecture for continuous blood pressure estimation using attention mechanism," *Sensors*, vol. 20, no. 8, p. 2338, 2020.

[16] M. Panwar, A. Gautam, D. Biswas, and A. Acharyya, "Pp-net: A deep learning framework for ppg-based blood pressure and heart rate estimation," *IEEE Sensors Journal*, vol. 20, no. 17, pp. 10 000–10 011, 2020.

[17] D. Lee, H. Kwon, D. Son, H. Eom, C. Park, Y. Lim, C. Seo, and K. Park, "Beat-to-beat continuous blood pressure estimation using bidirectional long short-term memory network," *Sensors*, vol. 21, no. 1, p. 96, 2021.

[18] M. Liu, L.-M. Po, and H. Fu, "Cuffless blood pressure estimation based on photoplethysmography signal and its second derivative," *International Journal of Computer Theory and Engineering*, vol. 9, no. 3, p. 202, 2017.

[19] K. Takazawa, N. Tanaka, M. Fujita, O. Matsuoka, T. Saiki, M. Aikawa, S. Tamura, and C. Ibukiyama, "Assessment of vasoactive agents and vascular aging by the second derivative of photoplethysmogram waveform," *Hypertension*, vol. 32, no. 2, pp. 365–370, 1998.

[20] L. A. Bortolotto, J. Blacher, T. Kondo, K. Takazawa, and M. E. Safar, "Assessment of vascular aging and atherosclerosis in hypertensive subjects: second derivative of photoplethysmogram versus pulse wave velocity," *American journal of hypertension*, vol. 13, no. 2, pp. 165–171, 2000.

[21] P. Li and T.-M. Laleg-Kirati, "Central blood pressure estimation from distal ppg measurement using semiclassical signal analysis features," *IEEE Access*, vol. 9, pp. 44 963–44 973, 2021.

[22] Y. Kurylyak, F. Lamonaca, and D. Grimaldi, "A neural network-based method for continuous blood pressure estimation from a ppg signal," in *2013 IEEE International Instrumentation and Measurement Technology Conference (I2MTC)*, 2013, pp. 280–283.

[23] N. Hasanzadeh, M. M. Ahmadi, and H. Mohammadzade, "Blood pressure estimation using photoplethysmogram signal and its morphological features," *IEEE Sensors Journal*, vol. 20, no. 8, pp. 4300–4310, 2020.

[24] M. Radha, K. De Groot, N. Rajani, C. C. Wong, N. Kobold, V. Vos, P. Fonseca, N. Mastellos, P. A. Wark, N. Velthoven *et al.*, "Estimating blood pressure trends and the nocturnal dip from photoplethysmography," *Physiological measurement*, vol. 40, no. 2, p. 025006, 2019.

[25] Y. Zhang and Z. Feng, "A svm method for continuous blood pressure estimation from a ppg signal," in *Proceedings of the 9th international conference on machine learning and computing*, 2017, pp. 128–132.

[26] C.-T. Yen, J.-X. Liao, and Y.-K. Huang, "Applying a deep learning network in continuous physiological parameter estimation based on photoplethysmography sensor signals," *IEEE Sensors Journal*, vol. 22, no. 1, pp. 385–392, 2021.

[27] J. Leitner, P.-H. Chiang, and S. Dey, "Personalized blood pressure estimation using photoplethysmography: A transfer learning approach." *IEEE journal of biomedical and health informatics*, vol. PP, 2021.

[28] G. Slapničar, N. Mlakar, and M. Luštrek, "Blood pressure estimation from photoplethysmogram using a spectro-temporal deep neural network," *Sensors*, vol. 19, no. 15, p. 3420, 2019.

[29] O. Schlesinger, N. Vigderhouse, D. Eytan, and Y. Moshe, "Blood pressure estimation from ppg signals using convolutional neural networks and siamese network," in *ICASSP 2020 - 2020 IEEE International Conference on Acoustics, Speech and Signal Processing (ICASSP)*, 2020, pp. 1135–1139.

[30] Ics, "https://archive.ics.uci.edu/ml/datasets/cuffless+blood+pressure+estimation/," 2021.

[31] M. Kachuee, M. M. Kiani, H. Mohammadzade, and M. Shabany, "Cuffless high-accuracy calibration-free blood pressure estimation using pulse transit time," in *2015 IEEE international symposium on circuits and systems (ISCAS)*. IEEE, 2015, pp. 1006–1009.

[32] A. A. M. Instrumentation, "American national standards for electronic or automated sphygmomanometers," *ANSI/AAMI SP 10-1987*, 1987.

[33] E. O'Brien, J. Petrie, W. Littler, M. de Swiet, P. L. Padfield, K. O'Malley, M. Jamieson, D. Altman, M. Bland, and N. Atkins, "The british hypertension society protocol for the evaluation of automated and semi-automated blood pressure measuring devices with special reference to ambulatory systems." *Journal of hypertension*, vol. 8, no. 7, pp. 607–619, 1990.